α- and β-$La_4Ti_9Si_4O_{30}$: Synthesis and Structure of the Second Member ($m = 2$) of Novel Layered Oxosilicates Containing (110) Rutile Sheets. Electrical Property and Band Structure Characterization of the Mixed-Valence Titanium(III/IV) Oxosilicate Series, $La_4Ti(Si_2O_7)_2(TiO_2)_{4m}$ ($m = 1, 2$)

Shumin Wang,[†] Shiou-Jyh Hwu,*[,†] Jeffrey A. Paradis,[‡] and Myung-Hwan Whangbo*[,‡]

Contribution from the Department of Chemistry, Rice University, P.O. Box 1892, Houston, Texas 77251, and Department of Chemistry, North Carolina State University, Raleigh, North Carolina 27695-8204

Received December 19, 1994[⊗]

Abstract: Single crystals of two mixed-valence lanthanum titanium(III/IV) oxosilicates, α- and β-$La_4Ti_9Si_4O_{30}$, were grown by a high-temperature, solid-state reaction employing $BaCl_2$ molten salt. Their structures were determined by single crystal X-ray diffraction methods. Both phases crystallize in a monoclinic lattice, *C2/m* (No. 12), with $a = 13.545(2)$ Å, $b = 5.751(1)$ Å, $c = 15.1888(9)$ Å, $\beta = 110.922(7)°$, and $V = 1105.1(3)$ Å^3 for α-$La_4Ti_9Si_4O_{30}$ and $a = 13.536(2)$ Å, $b = 5.750(1)$ Å, $c = 14.252(1)$ Å, $\beta = 95.387(8)°$, and $V = 1104.4(3)$ Å^3 for β-$La_4Ti_9Si_4O_{30}$ with $Z = 2$. These phases are polymorphs which represent the second member ($m = 2$) of the layered oxosilicate series, $La_4Ti(Si_2O_7)_2(TiO_2)_{4m}$. The two-dimensional framework can be viewed as a rutile lattice, TiO_2, that is sliced by closed-shell, nonmagnetic silicate slabs, $La_4Ti(Si_2O_7)_2$, along the (110) plane at various octahedra thicknesses, m. The physical and electronic properties of this layered compound series were characterized by measuring their electrical resistivities and calculating their electronic band structures with the extended Hückel tight-binding (EHTB) method. The bulk resistivity showed semiconducting behavior with small gap energies. When the temperature is lowered, the $m = 1$ and 2 phases exhibit a sharp resistivity increase below ~20 and ~80 K, respectively. The EHTB calculations reveal that the d electrons of the $La_4Ti(Si_2O_7)_2(TiO_2)_{4m}$ ($m = 1, 2$) phases reside not in the silicate slabs but in the (110) rutile layers, and the bottom portions of their d-block bands are partially filled. The observed sharp resistivity transition requires a localization of the electrons in the partially filled rutile band. The nonmetallic state of these quasi-two-dimensional compounds is probably caused by a bipolaron formation not be electron–electron repulsion or random potential. In this paper, the results from the EHTB calculations and the bond valence sum analysis are contrasted with regard to charge distribution.

1. Introduction

Over the years much attention has been devoted to mixed-valence transition metal oxides that exhibit electronic instabilities such as superconductivity, charge density waves, and magnetic ordering.[1-6] These metal oxides have an important electronic feature that their metal cations possess partially filled d orbitals. When these orbitals overlap through direct metal–metal contacts to give wide d-block bands, the oxides become metallic, as found for early transition metal monoxides (e.g., TiO and VO in rock-salt structure).[6] The partially-filled d-block bands of such compounds have primarily metal d-orbital character. In the vast majority of oxides with late transition metals, both metal d and oxygen p orbitals contribute significantly to the partially-filled d-block bands, and the metal ions interact through the metal–oxygen–metal bridges, as found for the cuprate superconductors[5] and molybdenum and tungsten oxides.[6] Most of these oxides have distorted coordination geometries that are a direct effect of the electronic interactions associated with transition metal centers.

Structurally, the arrangement of oxygen (O) atoms about transition metal (M) centers facilitates different types of bond interactions. Many transition metal oxide structures are built up of fused MO_6 octahedra by sharing their vertices, edges, or faces.[8,9] The corner-shared octahedral structure is characterized uniquely by metal–oxygen–metal (M–O–M) interactions, whereas the face-sharing structure is dominated by metal–metal (M–M) interactions. In the edge-sharing structure, both M–M and M–O–M interactions are important for the delocalization of conducting electrons which gives rise to metallic conductivity. In a compound with a reduced O/M ratio, which is necessary

[†] Rice University.
[‡] North Carolina State University.
[⊗] Abstract published in *Advance ACS Abstracts*, May 15, 1995.

(1) Goodenough, J. B. In *Progress in Solid State Chemistry*; Reiss, H., Ed.; Pergamon Press: New York, 1971; p 145.
(2) Wilson, J. A. *Adv. Phys.* **1972**, *21*, 143.
(3) (a) *Chemistry of High-Temperature Superconductors*; Nelson, D. L., Whittingham, M. S., George, T. F., Eds.; ACS Symposium Series 351; American Chemical Society: Washington, DC, 1987. (b) *Chemistry of High-Temperature Superconductors II*; Nelson, D. L., George, T. F., Eds.; ACS Symposium Series 377; American Chemical Society: Washington, DC, 1988.
(4) (a) Greenblatt, M. *Chem. Rev.* **1988**, *88*, 31. (b) Schlenker, C.; Dumas, J. In *Crystal Chemistry and Properties of Materials with Quasi-One-Dimensional Structures*; Rouxel, J., Ed.; D. Reidel Publishing Co.: The Netherlands, 1986; p 135. (c) Banks, E.; Wold, A. In *Preparative Inorganic Reactions*; Jolly, W. L., Ed.; Wiley: New York, 1968; Vol. 4, pp 237. (d) Hagenmuller, P. *Prog. Solid State Chem.* **1971**, *5*, 71.
(5) Whangbo, M.-H.; Torardi, C. C. *Acc. Chem. Res.* **1991**, *24*, 127.
(6) (a) Canadell, E.; Whangbo, M.-H. *Chem. Rev.* **1991**, *91*, 965. (b) Canadell, E.; Whangbo, M.-H. *Inorg. Chem.* **1994**, *33*, 1864.
(7) Howe, A. T.; Fenshaw, P. J. *Q. Rev.* **1967**, *21*, 507.
(8) Wells, A. F. *Structural Inorganic Chemistry*, 5th ed.; Oxford University Press: New York, 1984.
(9) Raveau, B. *Rev. Inorg. Chem.* **1987**, *9*, 37.

0002-7863/95/1517-5515$09.00/0

to condense the MO_6 octahedra, metal clusters with extended M−M bonding begin to form.[10]

Investigation of transition metal silicates and phosphates has revealed a large collection of structural families with little correlation to the known structural types adopted by above referenced transition metal oxide compounds. This is attributed to the unique bonding nature of the tetrahedrally coordinated silicon and phosphorus with oxygens, forming oxy anions, e.g., XO_4^{n-} and $X_2O_7^{m-}$ ($X = Si^{4+}$, P^{5+}; $n = 4, 3$; $m = 6, 4$, respectively). The bonding of these anions can be considered "omnidirectional"; in contrast to the monatomic oxide anions, silicates and phosphates are polyanions whose terminal oxygens are available for bonding with transition metal cations in a variety of ways to form a large class of structurally complex compounds. Given the fact that layered structures are often observed in binary compounds containing polarizable, heavy anions, such as chalcogenides and halides, but rarely in oxides, the polarizable silicate and phosphate oxy anions with their flexible X−O bonding may facilitate the formation of a layered framework.

In recent studies of reduced titanium phosphate synthesis, for example, several interesting framework structures containing discrete TiO_6 octahedra,[11] face-sharing Ti_2O_9 double octahedra,[12] and edge-sharing $[TiO_4]_\infty$ octahedral chains[13] have been discovered. These titanium octahedral structures are separated by phosphate groups, becoming electronically insulated due to the closed-shell, nonmagnetic nature of the phosphate anions.[11a] We notice that in these examples of mixed-framework (TiO_6/PO_4) compounds, isolated TiO_6 octahedron will result when the P/Ti ratio is high, e.g., $BaTi_2(P_2O_7)_2$, and higher degrees of fusion of octahedra (one-dimensional octahedral chains, for instance) will ensue when the P/Ti ratio is lowered, e.g., $TiPO_4$.

Low-dimensional solids of reduced transition metal compounds are of fundamental interest because of their anisotropic structural property and, especially, the associated electronic instability. The number of octahedral oxides with a layer structure is limited because it is rather difficult to ensure the rigidity of layers which are only built up from octahedra; this is particularly true for structures having layers which are one or two octahedra thick.[9] A family of newly discovered oxosilicate compounds has shown a novel feature in that thin two-dimensional transition metal oxide structures are intergrown with the silicate lattice as a backbone. Compounds synthesized, thus far, showing novel structural features are one-dimensional $(Ba_3Nb_6Si_4O_{26})_n(Ba_3Nb_8O_{21})(n = 1-4)$ series,[14] $La_2Ti_2SiO_9$,[15] and two-dimensional $[(RE)_4M(Si_2O_7)_2](MO_2)_{4m}$ series (RE = La, Nd, M = Ti and RE = La, M = V for $m = 1$; RE = La, M = Ti for $m = 2$).[12,16-17] The crystal structure analysis shows $La_4Ti_5Si_4O_{22}$ to be the first member ($m = 1$) of the $[La_4Ti(Si_2O_7)_2](TiO_2)_{4m}$ series, which is the first reported structure of the layered chevkinite mineral.[17] The synthesis and structure of the second member ($m = 2$) of the series, $La_4Ti_9Si_4O_{30}$, were briefly discussed.[16] Further structural studies of the $La_4Ti_9Si_4O_{30}$ phase have revealed the existence of a second polymorph, whose structure is named as the β form, while the previously reported perrierite-related $La_4Ti_9Si_4O_{30}$ phase is now referred to as the α form. In the present work, we described in detail molten-salt synthesis, single crystal structures and offer a comparison of the α- and β-$La_4Ti_9Si_4O_{30}$ phases. The electrical property and band structure of this mixed-valence titanium(III/IV) oxosilicate series, $La_4Ti(Si_2O_7)_2(TiO_2)_{4m}$ ($m = 1, 2$), are discussed in terms of the electronic interactions in a confined space with respect to the (110) rutile sheets.

2. Synthesis and Structure Characterization of α- and β-$La_4Ti_9Si_4O_{30}$

Synthesis. As reported earlier,[16,17b] it is difficult to prepare single crystals of transition metal oxosilicate compounds of $La_4Ti(Si_2O_7)_2(TiO_2)_{4m}$ ($m = 1, 2$) by using a traditional solid-state method. This is attributed to the refractory nature of the binary oxide reactants. For example, the melting points of La_2O_3 and Ti_2O_3 are 2307 and 2310 °C, respectively. Thus, a halid flux was employed in our exploratory synthesis to grow single crystals for structure and property characterization. For the synthesis of the title compounds, a reaction originally intended to prepare transition metal-rich, phosphate-based phases was loaded in the ratio of reactants La_2O_3:Ti_2O_3:P_2O_5 = 1:3:1. In a typical reaction, a load of ca. 0.5 g was used, which contains 0.1812 g of La_2O_3 (Aldrich, 99.99%), 0.2398 g of Ti_2O_3 (Alfa, 99+%), and 0.0790 g of P_2O_5 (Mallinckrodt, 99+%). These reactants and ca. 2.5 g of barium chloride (dried from $BaCl_2{\cdot}2H_2O$, EMScience 99%, stored in drybox prior to use) were ground together inside a nitrogen-gas-purged drybox. The reaction mixture was then sealed in an evacuated silica tube, the inner surface of which was coated with carbon film by pyrolysis of acetone. The mixture was heated at 1100 °C for ca. 20 days and was followed by slow cooling to 800 °C at a rate of −25 °C/h and then furnace cooling to room temperature. The crystals (~10% in yield) were retrieved by washing with deionized water using suction filtration. During the reaction, the carbon coating was destroyed, and the quartz tube reacted. A microprobe analysis showed the presence of silicon (no phosphorus) in the crystal samples, and the quartz ampule was believed the source of silicon. A carbon-assisted reduction reaction concerning the incorporation of silicate anion in the oxosilicate series was proposed in the previous report.[17b]

After the structure determination with all of the elements identified, a follow-up preparation of bulk quantity of the $m = 2$ phase was attempted by using stoichiometric amounts of reactants (La_2O_3:TiO_2:Ti_2O_3:SiO_2 = 1.0:2.5:1.0:2.0 mmol). The reactants were sealed in a fused silica tube with carbon coating (or else the quartz container was attacked), were heated at 1200 °C for 10 days, and were allowed to furnace cool to room temperature. This time the carbon coating remained intact. Powder X-ray diffraction (Philips PW 1840 diffractometer with Cu Kα radiation, λ = 1.5418 Å, and Ni filter) showed that the $m = 2$ phase was synthesized in a mixture of two polymorphs.

Crystal Structure Determination. Black, thin column crystals of α- and β-$La_4Ti_9Si_4O_{30}$ were selected for single crystal X-ray diffraction measurements with a Rigaku AFC5S four circle diffractometer, and diffraction data were collected at room temperature. The crystallographic data are summarized in Table 1. The unit cell parameters and the orientation matrix for data collection were determined by a least squares fit of 25 peak maxima with $7° < 2\Theta < 24°$. There was no detectable decay

(10) McCarley, R. E. In *Inorganic Chemistry Toward the 21st Century*; Chisholm, M. H., Ed.; ACS Symposium Series 211; American Chemical Society: Washington, DC, 1983; p 273.

(11) (a) Wang, S.; Hwu, S.-J. *J. Solid State Chem.* **1991**, *90*, 31. (b) Wang, S.; Hwu, S.-J. *J. Solid State Chem.* **1991**, *90*, 377. (c) Wang, S.; Hwu, S.-J. *J. Solid State Chem.* **1991**, *92*, 219. (d) Wang, S.; Hwu, S.-J. *Chem. Mater.* **1992**, *4*, 589. (e) Wang, B.; Greenblatt, M.; Wang, S.; Hwu, S.-J. *Chem. Mater.* **1993**, *5*, 23.

(12) Wang, S. Ph.D. Dissertation, Rice University, 1993.

(13) (a) S. Wang, unpublished research, Rice University, Houston, TX, 1990. (b) Kinomura, N.; Muto, F.; Koizumi, M. *J. Solid State Chem.* **1982**, *45*, 252.

(14) (a) Serra, D. L.; Hwu, S.-J. *J. Solid State Chem.* **1992**, *101*, 32. (b) Serra, D. L. Ph.D. Dissertation, Rice University, 1994.

(15) Benbertal, D.; Mosset, A.; Trombe, J. C. *Mater. Res. Bull.* **1994**, *29*, 47.

(16) Wang, S.; Hwu, S.-J. *J. Am. Chem. Soc.* **1992**, *114*, 6920.

(17) (a) Chen, S. C.; Ramanujachary, K. V.; Greenblatt, M. *Inorg. Chem.* **1994**, *33*, 5994. (b) Wang, S.; Hwu, S.-J. *Inorg. Chem.* **1995**, *34*, 166.

Table 1. Crystallographic Data[a] for α- and β-$La_4Ti_9Si_4O_{30}$

chemical formula	α-$La_4Ti_9Si_4O_{30}$	β-$La_4Ti_9Si_4O_{30}$
fw	1579.05	1579.05
a, Å	13.545(2)	13.536(2)
b, Å	5.751(1)	5.750(1)
c, Å	15.1888(9)	14.252(1)
β, deg	110.922(7)	95.387(8)
V, Å^3	1105.1(3)	1104.4(3)
Z	2	2
space group	$C2/m$ (No. 12)	$C2/m$ (No. 12)
T, °C	295	295
λ,	0.710 69	0.710 69
ϱ_{calcd}, g cm^{-3}	4.75	4.75
linear abs coeff, cm^{-1}	109.68	109.74
R^b	0.021	0.025
R_w[c]	0.031	0.041

[a] The refinement of cell constants is constrained in the monoclinic crystal system. [b] $R = \sum[|F_o| - |F_c|]/|\sum|F_o|$. [c] $R_w = [\sum w[|F_o| - |F_c|]^2/\sum w|F_o|^2]^{1/2}$.

during the data collection, according to the intensities of three standard reflections (α 1,−1,−1, 1,−1,−2, 0,0,−4; β 310, 1,1,−1, 110), which were measured every 150 reflections. The structure solution was carried out using the TEXSAN software package.[18] Data reduction, intensity analysis, and extinction conditions were determined with the program PROCESS. On the basis of the extinction conditions and the successful solution and structure refinement, the space group was determined to be $C2/m$ (No. 12). Lorentz−polarization and empirical absorption corrections based on three computer-chosen azimuthal scans (2Θ = 14.20, 14.49, 28.62° for α and β) were applied to the intensity data. The atomic coordinates of heavy atoms were determined using the SHELX-86 program.[19] The oxygen atoms were located by the consecutive calculations of difference Fourier maps. The structures and displacement parameters were then refined by the full-matrix least squares methods. The final atomic coordinates and thermal parameters are given in supplementary Tables SII and SIII.

3. Structural Characteristics of $La_4Ti(Si_2O_7)_2(TiO_2)_{4m}$ (m = 1, 2)

Figure 1 shows a schematic representation illustrating the layered nature of the $La_4Ti(Si_2O_7)_3(TiO_2)_{4m}$ (m = 1, 2) oxosilicate series. The frameworks of this compound series are quasi-two-dimensional containing single-sheet (m = 1) and double-sheet (m = 2) titanium oxide slabs. Because the adopted slab structure resembles the (110) plane of the tetragonal rutile lattice (see below), the TiO_2 layers will be referred to as the rutile slab, and for the simplicity of our discussion, the $La_4Ti(Si_2O_7)_2$ sublattice will be referred to as the silicate slab. This interesting feature of an intergrown lattice reminds us of the Aurivilius-type copper oxide high-T_c superconductors, in that the perovskite-type CuO_2 layers are intergrown with rock-salt-type MO (e.g., M = La, Sr, Ba, Bi, Tl, Hg) layers.[20] Electronically, the rock-salt sublattice in cuprates and, similarly, the silicate slab in this oxosilicate series serve as a charge reservoir to their corresponding oxide frameworks. Nevertheless, the low dimensionality with respect to the transition metal oxide framework has prompted us to investigate the structure/property correlation of the oxosilicate series by means of electrical property and band structure characterizations.

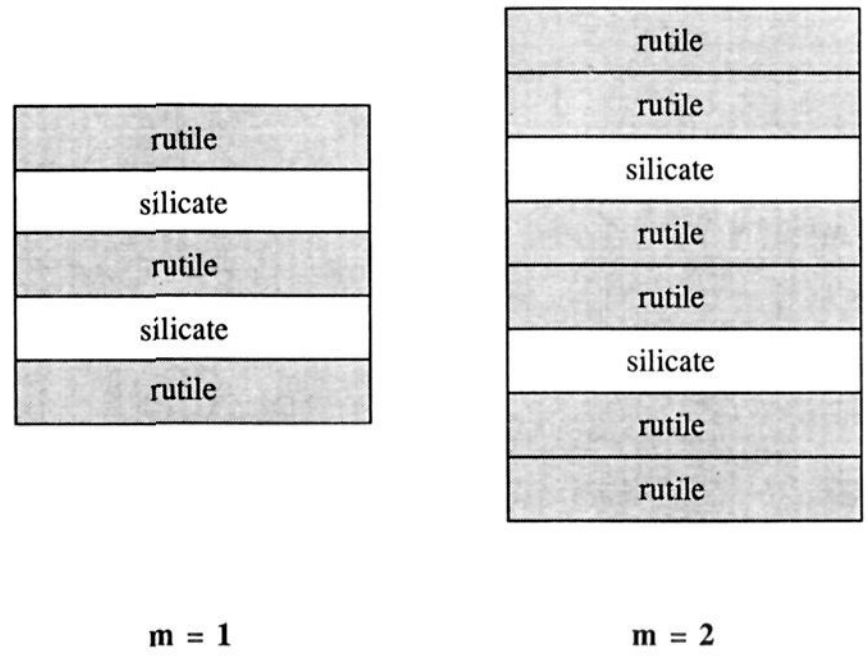

Figure 1. Schematic representations of the layered $La_4Ti(Si_2O_7)_2(TiO_2)_{4m}$ oxosilicate series containing single-sheet (m = 1) and double-sheet (m = 2) rutile (TiO_2) slabs.

The $La_4Ti(Si_2O_7)_2(TiO_2)_{4m}$ (m = 1, 2) phases are novel in the sense that their structures contain one (m = 1) and two (m = 2) octahedra thick, rutile-type titanium oxide layers, which are quite rare. Most layered transition metal oxides adopt perovskite or 1T-MX_2 type structures that possess close-packed oxide lattices.[5,6,8] In rutile, where the oxide layers are distorted in a so-called primitive tetragonal packed (ptp) array,[21] the TiO_6 octahedra are edge-shared along the octahedral chain corner-shared between the parallel chain. The characteristic features are 2-fold: (1) each oxygen atom is three-way sharing with titanium centers; (2) the parallel $[TiO_4]_\infty$ octahedral chains are orthogonal with respect to their equatorial planes.

As shown in the unit cell ORTEP[22] drawings (Figure 2) of the title compounds, α- and β-$La_4Ti_9Si_4O_{30}$, the titanium oxide slabs (outlined by the thick Ti−O bonds) alternate with the lanthanum titanium silicate slabs stacking along the crystallographic c axis. Four crystallographically independent titanium cations, one (Ti(1)) in the silicate slab and three (Ti(2−4)) in the rutile slab, are in TiO_6 octahedral coordination, while two silicon cations, Si(1) and Si(2), are in SiO_4 tetrahedral coordination geometries. The oxygen atoms in the rutile slab are three-coordinated except the ones at the interface, O(8) and O(9). The framework of the silicate slab is composed of one corner-shared TiO_6 octahedron per six Si_2O_7 pyrosilicate groups, accompanied by four lanthanum atoms (in two asymmetric crystallographic sites) to give rise to the structural formula $[La_4Ti(Si_2O_7)_2] \equiv [La_4Ti(Si_2O_7)_{6/3}]$. The lanthanum cations, La^{3+}, reside in the channels near the interface in a geometry best described as a bicapped trigonal prism (btp) made of eight oxygen atoms, LaO_8. It is noted that these polymorphic structures are closely related to the previously reported framework of the m = 1 phase[17] in terms of above discussed bond interactions, local geometries, and especially intergrowth sequence. In the following discussions, therefore, in addition to describing the interesting features of structure and bonding of the polymorphs, we will focus on the special phenomena associated with lattice matching and structural/electronic instability of the two-dimensional rutile sublattices.

(18) *TEXSAN: Single Crystal Structure Analysis Software, Version 5.0*; Molecular Structure Corp.: The Woodlands, TX, 1989.

(19) Sheldrick, G. M. *Crystallographic Computing 3*; Sheldrick, G. M., Krüger, C., Goddard, R., Eds.; Oxford University Press: New York, 1985; p 175.

(20) (a) Sheng, Z. Z.; Hermann, A. M.; El Ali, A.; Almason, C.; Estrada, J.; Datta, T.; Matson, R. *J. Phys. Rev. Lett.* **1988**, *60*, 937. (b) Torardi, C. C. Subramanian, M. A.; Calabrese, J. C.; Gopalakrishnan, J.; Morrissey, K. J.; Askew, T. R.; Flippen, R. B.; Chowdhry, U.; Sleight, A. W. *Science* **1988**, *240*, 631. (c) Schilling, A.; Cantoni, M.; Guo, J. D.; Ott, H. R. *Nature* **1993**, *363*, 56. (d) Chmaissem, O.; Huang, Q.; Putilin, S. N.; Marezio, M.; Santoro, A. *Physica C* **1993**, *212*, 259.

(21) *Solid State Chemistry and Its Applications*; West, A. W., Ed.; John Wiley & Sons: New York, 1984; p 225.

(22) Johnson, C. K. *ORTEP II*; Report ORNL-5138; Oak Ridge National Laboratory: Oak Ridge, TN, 1976.

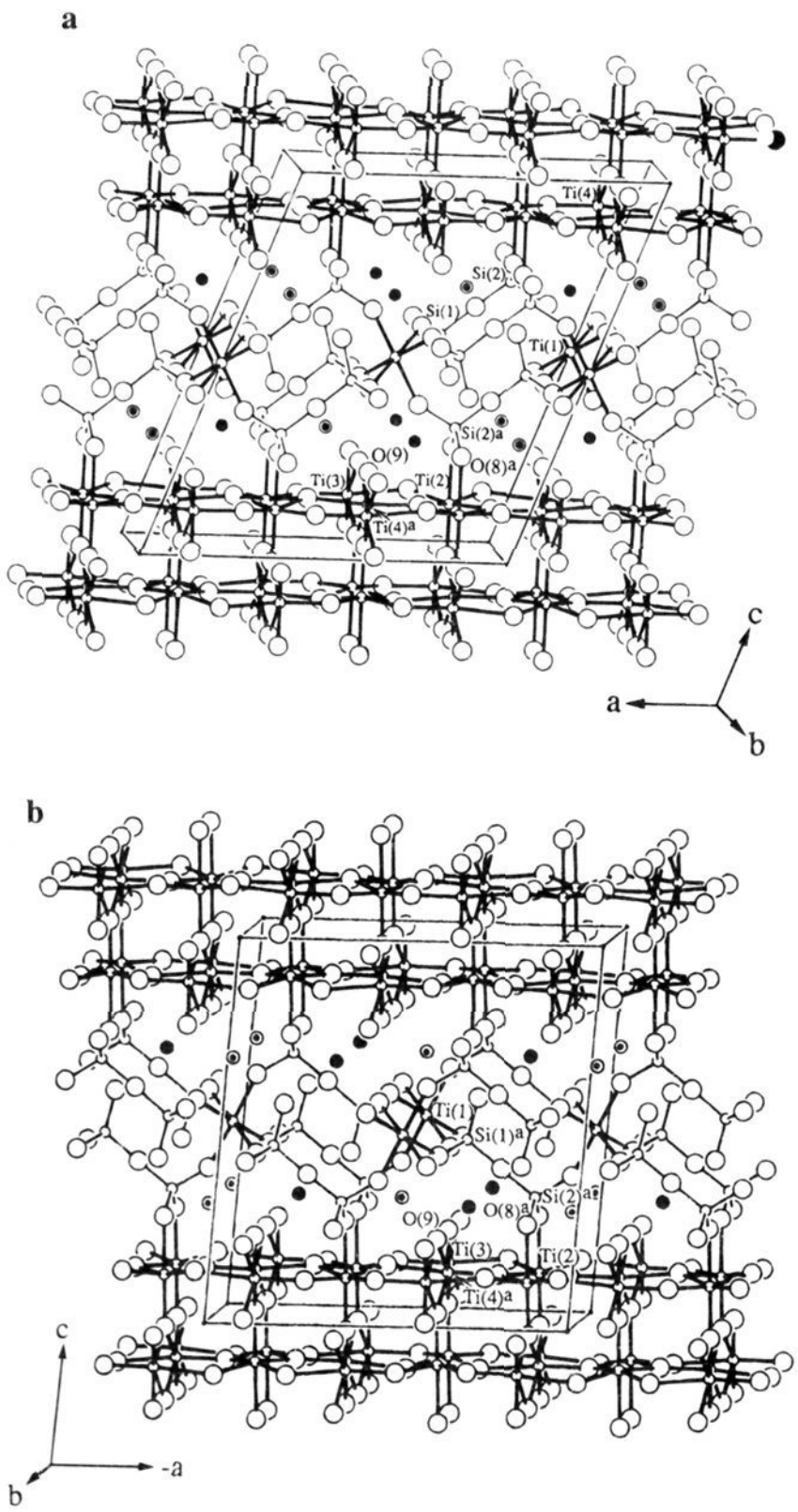

Figure 2. ORTEP drawings of unit cells of (a) α- and (b) β-$La_4Ti_9Si_4O_{30}$ viewed approximately along the *b* axis. The TiO_6 and Si_2O_7 polyhedra are outlined by thick and thin lines, respectively. The cations are presented by small circles (La(1)/La(2), dotted/solid circles; Ti, Si, open circles), and oxygen anions are large circles. a: $^1/_2 - x$, $^1/_2 + y$, $1 - z$.

The structures of these two new polymorphs are diastereomeric with respect to the relative orientations of two sublattices. While the layered orientation of the rutile slabs is fixed, as shown in Figure 2, the silicate sublattices in the α and β structures are mirror images of each other. The observed difference in the unit cell dimension *c* and monclinic angle β is a result of the alternation of lattice intergrowth between the rutile and silicate sublattices. Taking into account the tilted angle β, the d_{001} spacing ($\equiv c \sin \beta$), however, is essentially the same, e.g., 14.187 and 14.189 Å, respectively. Intuitively, the formation of the α and β phases is expected to be thermodynamically equivalent.

On the basis of the similar coordination geometries and chemical bonding, the two polymorphs are considered identical twins, and the difference in the two structures is essentially a matter of variation in the above mentioned lattice matching. To derive one structure from the other, one can physically disassemble the two sublattices along the planes of the interface

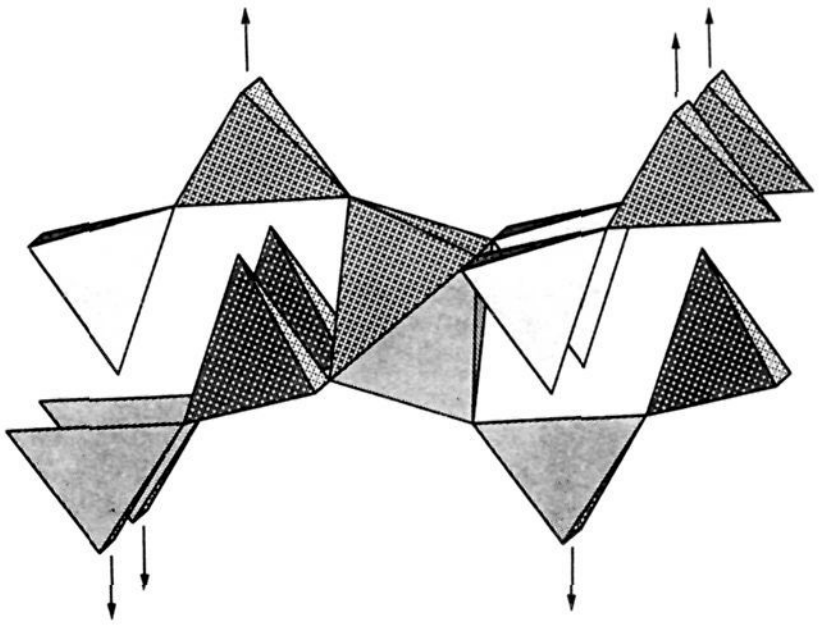

Figure 3. Polyhedral representation of the $Ti(1)(Si_2O_7)_6$ unit. The octahedron is centered by Ti, and each tetrahedron is centered by Si. The arrows are pointing into the rutile layers (see text).

Table 2. Spacing of the Rutile Chain, *a*/2, and the Bond Angle Si(1)−O−Si(2) of the $La_4Ti(Si_2O_7)_2(TiO_2)_{4m}$ Series

	a/2, Å	Si(1)−O−Si(2), deg
$La_4Ti_5Si_4O_{22}$ ($m = 1$)	6.811	177.9(4)
α-$La_4Ti_9Si_4O_{30}$ ($m = 2$)	6.773	178.7(4)
β-$La_4Ti_9Si_4O_{30}$ ($m = 2$)	6.768	179.0(4)

oxygen atoms, O(8) and O(9), and reassemble them according to the relative orientation discussed above. The periodicity of the octahedral chain ($d_{O(8)-O(8)} = a/2$), a critical parameter that measures proper lattice matching, is similar in the two structures, e.g., 6.773 Å (α) and 6.768 (β). In comparison, these distances are longer than 6.497 Å, that of the 3D tetragonal rutile lattice ($a = 4.594$ Å, $c = 2.958$ Å). This suggests that, sterically and electronically, the incorporated lanthanum cation provides the necessary expansion in repeating distances of the double-sheet rutile slab to facilitate a better matching with the silicate slab.

In the formation of the 3D lattice, the $Ti(1)(Si_2O_7)_6$ unit in the silicate slab serves as an unusual function to link the (110) rutile sheets together. This titanium-centered hexakis(pyrosilicate) unit can be considered a bulky ligand that chelates the rutile layers on the top and bottom of the octahedral layers. In Figure 3, the unit structure is viewed approximately along the *b* axis like in the unit cell so that all the chelating corners of the six pyrosilicates are shown pointing away from the titanium center, as indicated by the arrows. Due to the bond interaction of corner-shared TiO_6 and Si_2O_7 groups, the $Ti(1)(Si_2O_7)_6$ framework is adaptive, favoring the above discussed lattice matching. The parallel pyrosilicate groups provide additional flexibility to the lattice. It is interesting to note that, in Table 2, the Si(1)−O−Si(2) bond angles show a cooperative correlation with the above described lattice matching parameter; *a*/2; i.e., the wider the periodic spacing the larger the deviation of the angle from 180°.

The structural distortion due to lattice matching is extended to the rutile framework with respect to the octahedral tilting, similar to that seen in the tetragonal rutile lattice. In Figure 4, a close view of the partial structure of the double-sheet rutile slab is demonstrated by the $[(TiO_2)_4]_\infty$ network composed of Ti(2) and Ti(3)/Ti(4) octahedral chains. The extended double-sheet rutile slab is made up of fused $[(TiO_2)_4]_\infty$ units, each of which is centered around the 2-fold axis of the unit cell. With respect to the edge-sharing "planes" (the "equatorial planes") of the octahedral chains, the adjacent chains are orthogonal to each other and are fused together by corner sharing (Figure 4b). In the tetragonal rutile structure, the parallel octahedral chains

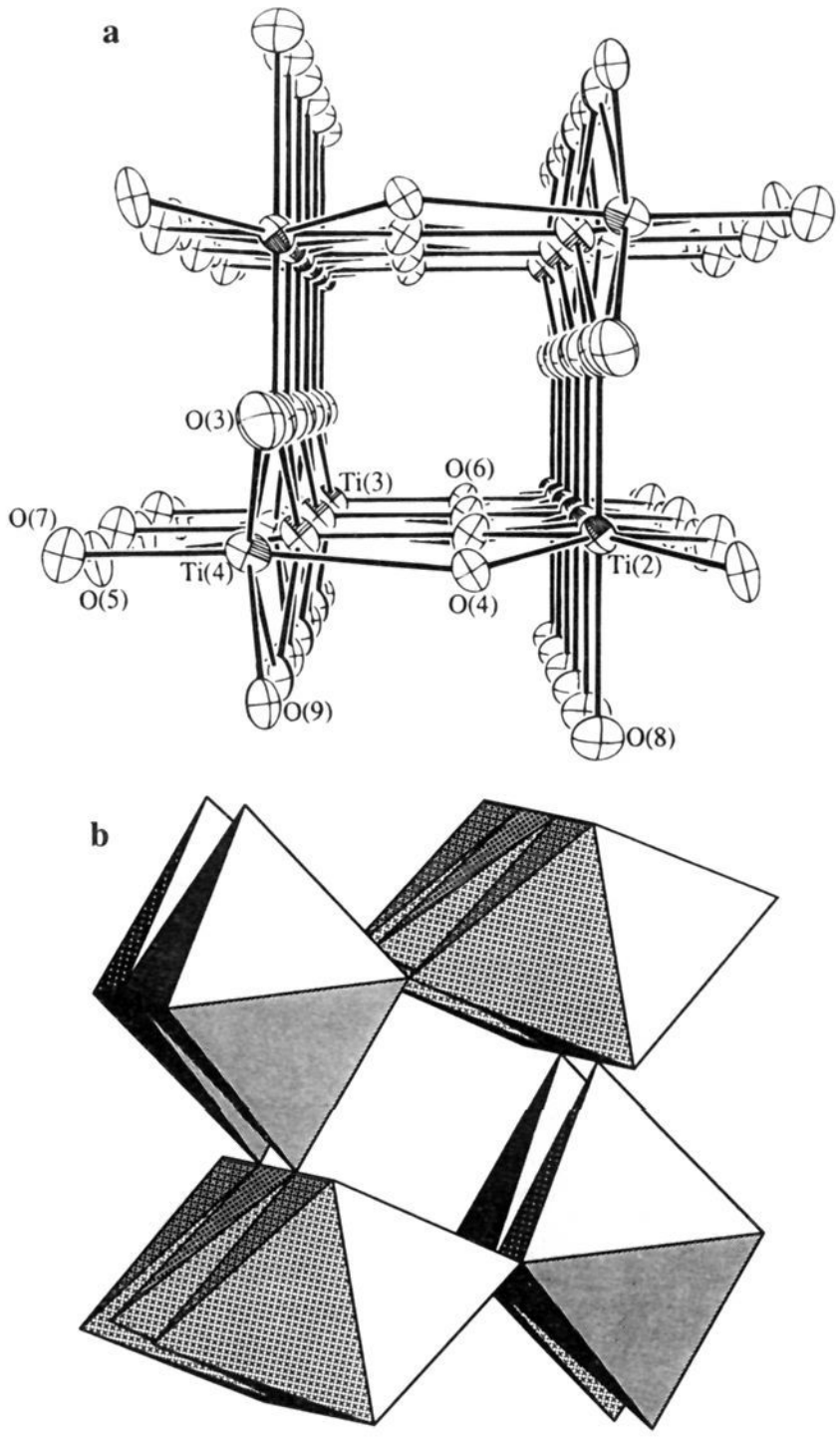

Figure 4. $[(TiO_2)_4]_\infty$ network, a partial structure of the double-sheet rutile slab, shown by (a) the ORTEP drawing of the perspective view with anisotropic atoms being presented at 90% probability, and (b) the polyhedral representation of the extended octahedral chains.

are slightly tilted such that the equatorial planes deviate from orthogonal orientation, and the titanium centers of octahedral chains remain linear. In contrast to the tetragonal rutile lattice, the network structure of the presently studied frameworks is characterized by an octahedral distortion along the chain, resulting in the zigzag Ti(3)/Ti(4) arrangement along with the linear Ti(2) centers. The polyhedral drawing shows that the equatorial planes are puckered in the Ti(2) chain and twisted along the Ti(3)/Ti(4) chain.

The octahedral distortion described above includes the close Ti−Ti bond interactions along octahedral chains. Figure 5 shows the edge-shared TiO_6 octahedral chains of Ti(2), top, and Ti(3)/Ti(4), bottom, parallel to the crystallographic *b* axis. As expected, short Ti−Ti distances are observed due to the edge-shared octahedral arrangement, e.g., 2.76−3.00 Å (α) and 2.76−2.99 Å (β). The smaller Ti−Ti distances are shorter than 2.96 Å of the tetragonal rutile structure[1] and 3.02 Å of the critical distance for the Ti−Ti interaction.[23] These short Ti−Ti distances are associated with an alternating short-and-long Ti(2)−Ti(2) distances, e.g., 2.76/3.00 Å for α and 2.76/2.99 Å for β. The Ti(3)/Ti(4) chain, on the other hand, has a uniform Ti(3)−Ti(4) bond (2.91 Å for both forms). These inhomogeneous bond interactions are in fact different than what is observed in the $m = 1$ structure where all the Ti−Ti bond distances [i.e., Ti(2)−Ti(2) and Ti(3)−Ti(4)] are equal (2.84 Å).[17] Nevertheless, the averaged Ti−Ti distances in both α and β frameworks are ca. 2.89 Å, which suggests that the overall bond interaction is comparable to that of the single-sheet rutile structure. However, the distortion resulting from the inhomogeneous Ti−Ti spacing is probably associated with the electronic instability of low-dimensional octahedral chains due to low-concentration conducting electrons.

(23) Goodenough, J. B. *Prog. Solid State Chem.* **1971**, *5*, 145.

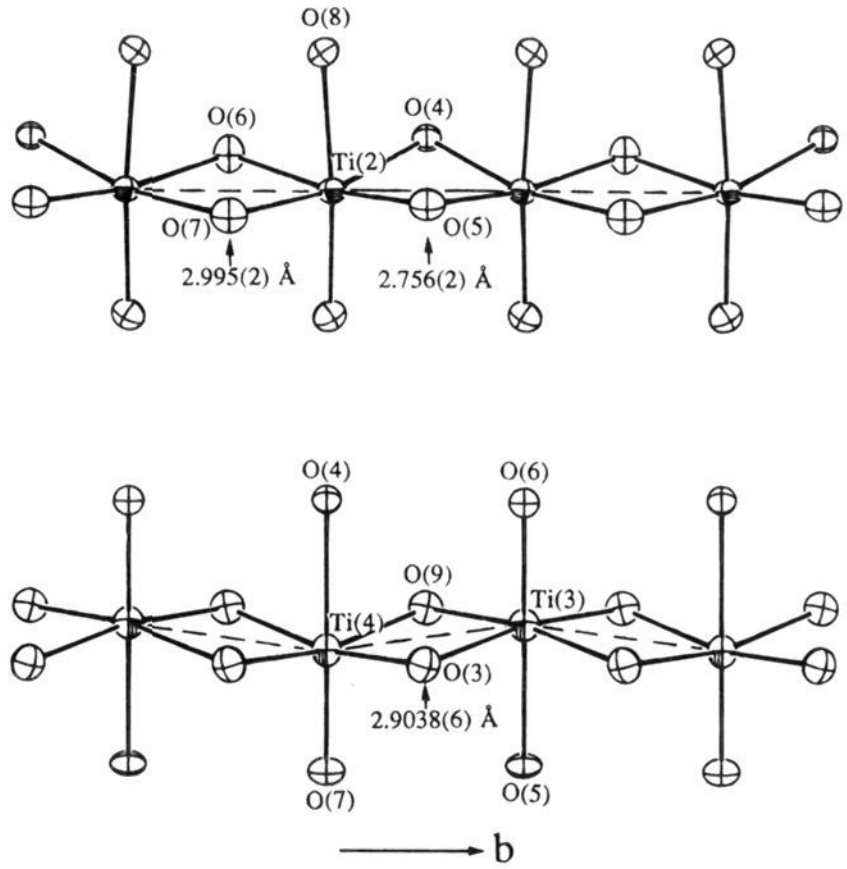

Figure 5. ORTEP drawing of the two octahedral chains of the α structure: Ti(2) chain (top) and Ti(3)/Ti(4) chain (bottom). The anisotropic atoms are presented at 90% probability. The bond distances are in angstroms.

4. Electrical Resistivities and Electronic Band Structures of $La_4Ti(Si_2O_7)_2(TiO_2)_{4m}$ ($m = 1, 2$)

Variable-temperature, four-probe dc resistivity measurements were performed on a pressed pellet sample of the mixed α and β phases.[24] The analysis of resistivity data is based on an assumption that the underlying electrical properties of these two polymorphs are identical as far as the rutile slabs are concerned. In Figure 6, the resistivity (ϱ) vs temperature (T) plot shows a semiconducting behavior with a small gap energy ($E_g = 0.25$ eV, derived from the corresponding $\ln(\varrho/\varrho_o)$ vs $1/T$ curve in the insert for the temperature range 130−300 K). The room-temperature (rt) resistivity is 2.5 Ω cm, and the resistivity increases sharply around 80 K. The ϱ vs T curve for the $m = 1$ phase[17] has similar features with respect to a semiconducting behavior and a small gap energy ($E_g = 0.13$ eV). For a comparison, the rt resistivity of the $m = 1$ phase is 8.8 Ω cm and the sharp resistivity transition is observed at 13 K. This is similar to observations made for the Aurivilius-type cuprate series,[20b] the thicker the conducting layer (rutile layers in this case) the lower the resistivity. Also the temperatures of the resistivity transition show an interesting trend, in that the double-sheet rutile compound has a higher transition temperature than the single-sheet compound. Caution must be taken in drawing

(24) The dimension of a pellet was approximately 12.0 × 3.0 × 0.2 mm. The current source used was 1 nA from 10 to 22 K and 1 μA from 24 to 300 K. The $I-V$ curves at both low-temperature and room-temperature ranges are linear.

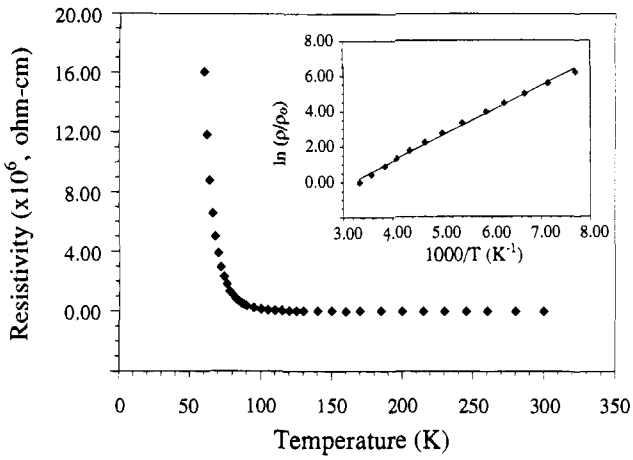

Figure 6. Resistivity (Ω m) *vs* temperature (K) plot of the pressed pellet samples of the mixture of α- and β-$La_4Ti_9Si_4O_{30}$. The corresponding $\ln(\varrho/\varrho_0)$ *vs* $1000/T$ (K^{-1}) plot is shown in the insert. The straight line is drawn to show the linearity.

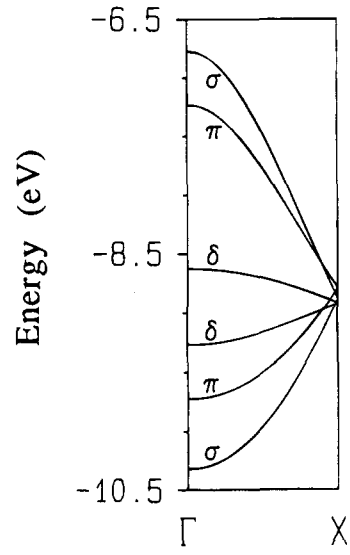

Figure 7. Dispersion relations of the t_{2g}-block bands calculated for an ideal edge-sharing octahedral TiO_4 chain (see text).

an absolute comparison, however, due to the complexity associated with the pressed pellet samples. In any event, all of these observations in electronic behavior can be rationalized by means of the following band structure analyses.

Band structure studies reveal that the oxosilicate series is quasi-one-dimensional with respect to the rutile chains. In the following paragraphs and sections 5 and 6, detailed investigations concerning the electronic interactions in a low-dimensional titanium oxide array and associated instability are discussed. First, Figure 7 shows the dispersion relations of the t_{2g}-block bands calculated, by employing the extended Hückel tight-binding (EHTB) method,[25] for an ideal edge-sharing octahedral chain made up of regular TiO_6 octahedra with Ti−O = 2.0 Å. The atomic parameters employed for our EHTB calculations are summarized in Table 3. For the ease of comparison with the electronic band structure of the $m = 1$ phase, $La_4Ti_5Si_4O_{22}$, the unit cell of the ideal octahedral chain was chosen to have two Ti atoms (i.e., Ti_2O_8). As described in detail elsewhere,[6a] the t_{2g}-block bands consist of σ, π, and δ bands. The σ and π bands are much wider than the δ band because the σ and π orbitals (**1** and **2**) provide a greater direct metal−metal overlap through the shared octahedral edges than do the δ orbitals (**3**).

(25) Whangbo, M.-H.; Hoffmann, R. *J. Am. Chem. Soc.* **1978**, *100*, 6093.

Table 3. Exponents ζ_i and the Valence Shell Ionization Potentials H_{ii} for Slater Type Atomic Orbitals χ_i[a,b]

atom	χ_i	ζ_i	ζ_i'	H_{ii} (eV)
O	2s	2.275		−32.3
O	2p	2.275		−14.8
Si	3s	1.383		−17.3
Si	3p	1.383		−9.2
Ti	4s	1.5		−8.97
Ti	4p	1.5		−5.44
Ti	3d	4.55 (0.4206)	1.40 (0.7839)	−10.8

[a] H_{ii}'s are the diagonal matrix elements $\langle\chi_i|H^{eff}|\chi_i\rangle$, where H^{eff} is the effective Hamiltonian. In our calculations of the off-diagonal matrix elements $H_{ij} = \langle\chi_i|H^{eff}|\chi_j\rangle$, the weighted formula was used: Ammeter, J. H.; Bürgi, H.-B.; Thibeault, J.; Hoffmann, R. *J. Am. Chem. Soc.* **1978**, *100*, 3686. [b] The 3d orbitals of Ti are given as a linear combination of two different Slater type orbitals, and each is followed by the weighting coefficient in parentheses.

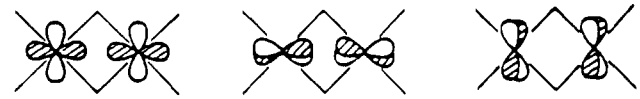

1 2 3

The dispersion relations of the bottom d-block bands calculated for the $m = 1$ phase, $La_4Ti_5Si_4O_{22}$, are shown in Figure 8a,[26] where the dashed line refers to the Fermi level appropriate for a normal metallic state. The total and projected density of states calculated for the $m = 1$ phase are shown in Figure 8b. Bands a and b are the σ bands of the octahedral chains containing the Ti(2) and the Ti(3)/Ti(4) atoms, respectively. Bands c and d are the π bands of the octahedral chains containing the Ti(3)/Ti(4) and Ti(2) atoms, respectively. As expected, the σ and π bands are dispersive only along the chain direction. Band e is the lowest-lying d-block band of the Ti(1) atoms in the silicate layer and is flat because the Ti(1) atoms are isolated. Band e lies above the Fermi level (i.e., the d-block bands of the Ti(1) atoms are not occupied) so that the oxidation state appropriate for Ti(1) is +4. This suggests an average oxidation state of +3 for the Ti(2), Ti(3), and Ti(4) atoms, if the oxidation states La^{3+}, O^{2-}, and Si^{4+} are adopted. This is consistent with the observation that the bottom portion of the σ and π d-block bands belonging to the Ti(2) and Ti(3)/Ti(4) atoms are partially filled. The bottom of the σ and π bands of the octahedral chains lies below the lowest-lying d-block band of Ti(1) because of the direct metal−metal bonding that occurs across the shared edges of the octahedral chains.

The dispersion relations of the bottom d-block bands calculated for the $m = 2$ phase, $La_4Ti_9Si_4O_{30}$, are similar to those of the $m = 1$ phase (hence not shown), except that the π bands are not occupied in the $m = 2$ phase.[26] The total and projected density of states calculated for the $m = 2$ phase are shown in Figure 9. As in the case of the $m = 1$ phase, the d-block bands of the Ti(1) atoms are not occupied, and the bottom portion of the d-block bands belonging to both the Ti(2) and the Ti(3)/Ti(4) atoms are partially filled. Thus, the oxidation state appropriate for the Ti(1) atoms is +4, which leads to an average oxidation state of +3.5 for the Ti(2), Ti(3), and Ti(4) atoms when the oxidation states La^{3+}, O^{2-}, and Si^{4+} are adopted.

5. Electron Localization in $La_4Ti(Si_2O_7)_2(TiO_2)_{4m}$ ($m = 1$, 2)

Our electronic band structure calculations predict that the silicate layers of both $m = 1$ and 2 phases contain Ti^{4+} (d^0)

(26) To simplify our EHTB calculations, the $m = 1$ phase $La_4Ti_5Si_4O_{22}$ was approximated by the $Ti_5Si_4O_{22}^{12-}$ lattice, and the $m = 2$ phase $La_4Ti_9Si_4O_{30}$ was approximated by the $Ti_9Si_4O_{30}^{12-}$ lattice.

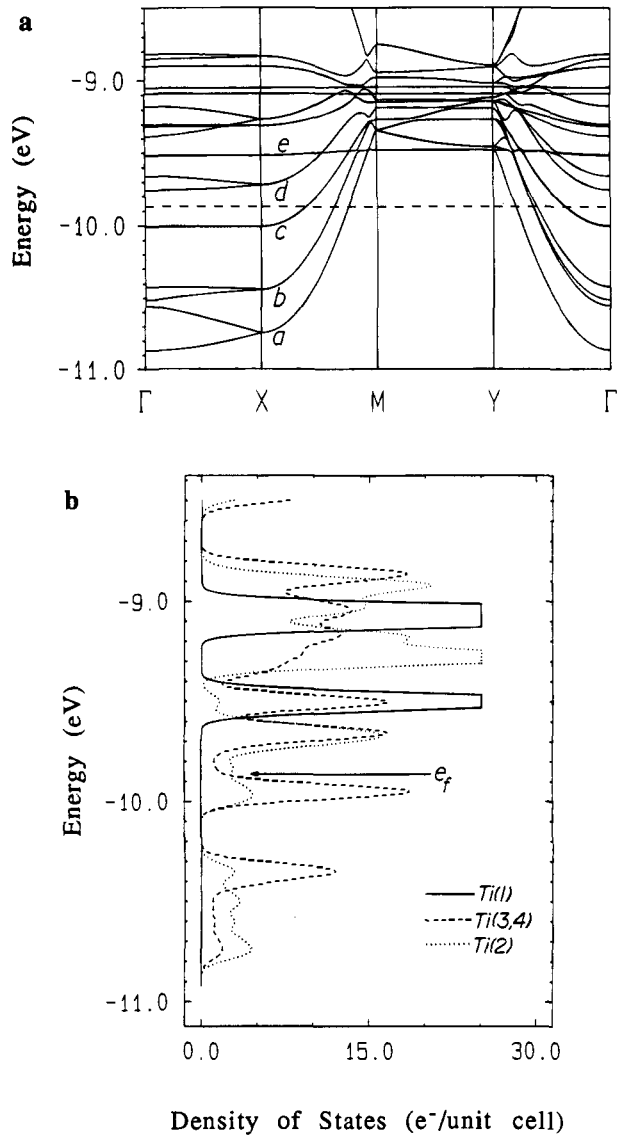

Figure 8. (a) Dispersion relations of the bottom portion of the d-block bands calculated for the $m = 1$ phase, $La_4Ti_5Si_4O_{22}$. $\Gamma = (0, 0, 0)$, $X = (a^*/2, 0, 0)$, $Y = (0, b^*/2, 0)$, and $M = (a^*/2, b^*/2, 0)$. (b) Total and projected density of states for the $m = 1$ phase, $La_4Ti_5Si_4O_{22}$.

ions and hence are diamagnetic. Since the bottom portions of the rutile layer d-block bands are partially filled, both $m = 1$ and 2 phases are predicted to be metallic, in contradiction to the results of the present electrical resistivity measurements. There are several electron-localization mechanisms by which a system with partially filled bands can become insulating. When the on-site repulsion (i.e., the pairing energy) is large compared to the widths of the partially filled bands, the electrons in these bands are localized to give rise to a magnetic insulating state.[27] For the $m = 1$ and 2 phases, the partially filled bands are quite wide, and so it seems unlikely that the electron localization is caused by the electron−electron repulsion mechanism. Electron localization can also be induced by random potentials, i.e., when the extent of the random potential fluctuation is large compared with the width of the partially filled band.[28] The crystal structures of the $m = 1$ and 2 phases determined by single crystal X-ray diffraction measurements indicate no disorder in their

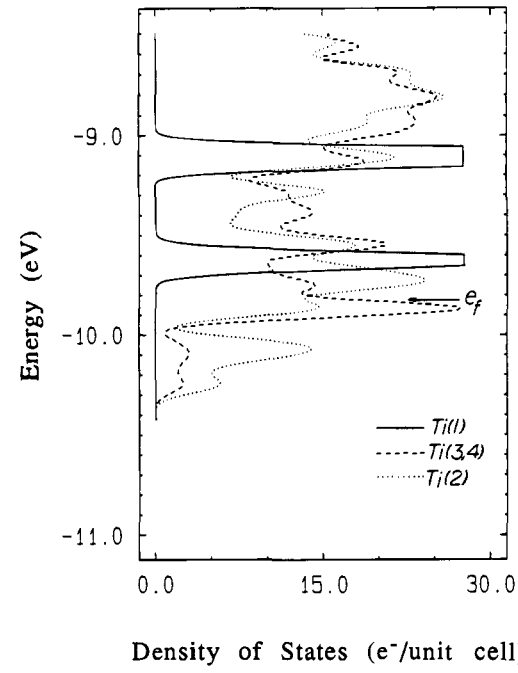

Figure 9. Total and projected density of states for the $m = 2$ phase, $La_4Ti_9Si_4O_{30}$.

atomic positions. Therefore, it is unlikely that the electron localization of the $m = 1$ and 2 phases is caused by the random potential mechanism.

For the $m = 1$ and 2 phases, the partially filled bands are wide, the carrier density is low, and the partially filled bands occur in the transition metal oxide framework containing a rutile structure. These situations are quite similar to those found in the titanium oxide Ti_4O_7, whose nonmetallic state below 150 K is associated with bipolaron formation,[29] i.e., electron pairing on adjacent Ti^{3+} sites to form $Ti^{3+}-Ti^{3+}$ pairs. By analogy, it is probable that the nonmetallic state of $La_4Ti(Si_2O_7)_2(TiO_2)_{4m}$ ($m = 1, 2$) is caused by a bipolaron formation in their rutile layers. To confirm this suggestion, it is necessary to grow large single crystals of $La_4Ti(Si_2O_7)_2(TiO_2)_{4m}$ ($m = 1, 2$) and measure their electrical resistivities and magnetic susceptibilities as a function of temperature.

6. Bond Valence Sum Analysis and Its Problem

The oxidation states of metal atoms are often estimated by calculating bond valence sums (BVS) on the basis of the observed metal−ligand bond lengths surrounding the metal atoms.[30] These calculations lead to the BVS values of 3.17 for Ti(1), 3.47 for Ti(2), 3.38 for Ti(3), and 3.41 for Ti(4), from which one might assign the oxidation state of +3 to the Ti(1) atom and an average oxidation state of +3.25 to the Ti(2), Ti(3), and Ti(4) atoms. Concerning the electronic structures of $La_4Ti_5Si_4O_{22}$, therefore, the BVS analysis presents a different picture from that given by the electronic band structure calculations, because it implies that each Ti(1) atom site carries an odd electron, and, hence, the silicate layer is paramagnetic. The BVS analysis assumes that the electron density lost by a metal atom is distributed only in the metal−ligand bonds surrounding it. Consequently, this analysis provides a misleading picture when there exist direct metal−metal bonding interactions as in

(27) (a) Mott, N. F. *Metal-Insulator Transitions*; Barnes and Noble: New York, 1977. (b) Brandow, B. H. *Adv. Phys.* **1977**, *26*, 651. (c) Whangbo, M.-H. *J. Chem. Phys.* **1979**, *70*, 4963.

(28) Anderson, P. W. *Phys. Rev.* **1958**, *109*, 1492. (b) Hayes, W.; Stoneham, A. M. *Defects and Defect Processes in Nonmetallic Solids*; Wiley: New York, 1985; Chapter 8.

(29) (a) Lakkis, S.; Schlenker, C.; Chakraverty, B. K.; Buder, R.; Marezio, M. *Phys. Rev. B* **1976**, *14*, 1429. (b) Chakraverty, B. K.; Schlenker, C. *J. Phys. (Les Ulis)* **1976**, *37*, C4−353. (c) Schlenker, C.; Marezio, M. *Phil. Mag. B* **1980**, *42*, 453.

(30) (a) Brown, I. D.; Altermatt, D. *Acta Crystallogr.* **1985**, *B41*, 244. (b) Brese, N. E.; O'Keefe, M. *Acta Crystallogr.* **1991**, *B47*, 192.

the $m = 1$ phase, $La_4Ti_5Si_4O_{22}$. For the $m = 2$ phase as well, the BVS analysis gives a picture in which the oxidation state of Ti(1) is +3,[16] because it neglects the effect of the direct metal−metal bonding interactions in the octahedral chains. The BVS analysis has also been found to provide erroneous conclusions on several other occasions.[31] In particular, the BVS analysis is strongly influenced by a steric factor, so that BVS values cannot be used as a measure of formal oxidation states unless the steric factor is constant, as found for various doped cuprate superconductors.[31a] This analysis is also found to be unreliable for those systems in which bond length variation is small, as in the case of monophosphate tungsten bronzes.[31b] Caution has to be exercised in the use of the BVS analysis.

7. Concluding Remarks

A new family of polymorphous α- and β-$La_4Ti_9Si_4O_{30}$ was discovered. Using a molten-salt flux method, new compounds $La_4Ti(Si_2O_7)_2(TiO_2)_{4m}$ ($m = 1, 2$) were isolated as single crystals. The molten-salt method seems to help overcome the difficulties encountered in a phase nucleation when refractory oxides are incorporated. The same method has also been successful in preparing mixed-metal chalcogenides.[32] Our electronic band structure calculations show that the d electrons of the title series reside not in the silicate layers but in the rutile layers, and the bottom portions of their d-block bands are partially filled. The conductivity measurements of press pellet samples of these oxosilicates show a semiconducting behavior with small gap energies and exhibit a sharp resistivity transition at a low temperature (around 13 and 80 K for the $m = 1$ and 2 phases, respectively). The electrons of these phases in their partially filled bands are localized. The electronic band and crystal structures of the $m = 1$ and 2 phases suggest that the bipolaron formation is likely to cause their electron localization. In terms of structure and bonding, the $m = 1$ and 2 phases are different than the titanium oxide Ti_4O_7, whose structure possesses a crystallographic shear (CS), made of face-sheared TiO_6 octahedra, at the interface of two rutile blocks.[33] Although CS is a structural phenomena commonly observed in reduced transition metal oxides, the (110) rutile sheets in the $La_4Ti(Si_2O_7)_2(TiO_2)_{4m}$ series are structurally isolated and electronically shielded by the silicate layers. Compounds of this kind are significant to the study of the behavior of conducting electrons in a confined space, where interlayer electron interactions are simplified.

Acknowledgment. Work at Rice University was supported by the National Science Foundation (Grant DMR-9208529), the Robert A. Welch Foundation, and the Exxon Education Foundation. Work at North Carolina State University was supported by the Office of Basic Energy Sciences, Division of Materials Sciences, U.S. Department of Energy, under Grant DE-FG05-86ER45259.

Supplementary Material Available: Tables of detailed crystallographic data, atomic coordinates, anisotropic thermal parameters, and important bond distances and angles, and profiles of calculated powder X-ray diffraction patterns of α- and β-$La_4Ti_9Si_4O_{30}$ (10 pages). This material is contained in many libraries on microfiche, immediately follows this article in the microfilm version of the journal, can be ordered from the ACS, and can be downloaded from the Internet; see any current masthead page for ordering information and Internet/access instructions.

JA9440819

(31) (a) Whangbo, M.-H.; Torardi, C. C. *Science* **1991**, *249*, 1143. (b) Canadell, E.; Whangbo, M.-H.; Rachidi, I. E.-I. *Inorg. Chem.* **1990**, *29*, 3871.

(32) (a) Carpenter, J. D.; Hwu, S.-J. *J. Solid State Chem.* **1992**, *97*, 332. (b) Carpenter, J. D.; Hwu, S.-J. *Chem. Mater.* **1991**, *4*, 1368. (c) Bucher, C.; Hwu, S.-J. *Inorg. Chem.* **1994**, *33*, 5831. (d) Hwu, S.-J.; Bucher, C. K.; Carpenter, J. D.; Taylor, S. P. *Inorg. Chem.* **1995**, *34*, 1979.

(33) Marezio, M.; Dernier, P. D. *J. Solid State Chem.* **1971**, *3*, 340.